Electronic Supplementary Information

Electrochemical Grafting of Organic Films on Silica

Zane Datson,[a] Essam Dief,[a] Tiexin Li,[a] Anton Le Brun,[b] Nadim Darwish*[a]

[a] School of Molecular and Life Sciences, Curtin Institute of Functional Molecules and Interfaces, Curtin University, Bentley, WA 6102, Australia.
[b] Australian Centre for Neutron Scattering, Australian Nuclear Science and Technology Organization (ANSTO), Lucas Heights, NSW 2234, Australia

Corresponding author email: nadim.darwish@curtin.edu.au

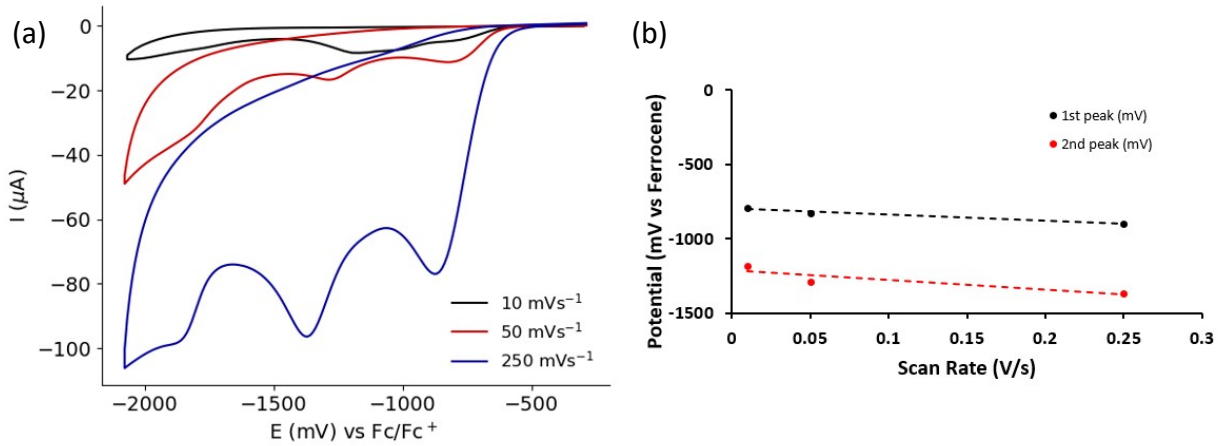

Fig S1. Reduction peak positions for electrochemical grafting of diazonium salts on nat–SiOx/Si as a function of the scan rate. (a) Cyclic voltammograms for the electrochemical grafting of **1** on nat–SiOx/Si at different scan rates (0.01 Vs^{-1} (black trace), 0.05 Vs^{-1} (red trace) and 0.25 Vs^{-1} (blue trace)). (b) Plot of reduction potential vs the scan rate, showing that the reducing potential appears more negative with increasing scan rates.

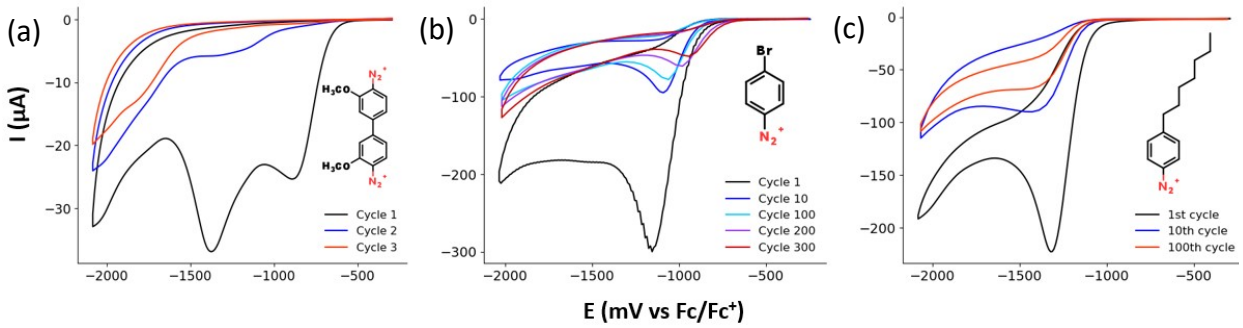

Fig S2. Plots showing the repeated voltametric cycling of the diazonium molecules on nat–SiOx/Si until the organic film is thick enough to block further reduction for (a) **1**, (b) **2** and (c) **3**.

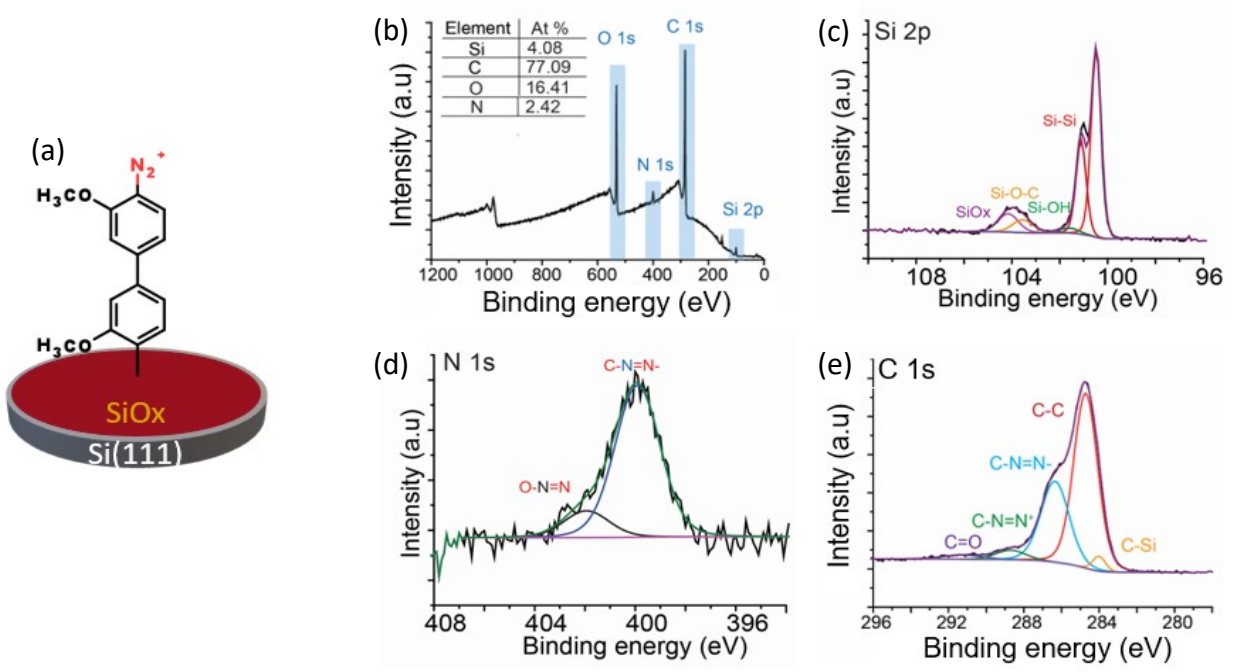

Fig S3. Schematic showing all XPS spectra collected for **1** on nat–Si/SiOx. (a) A schematic showing **1** attached to a nat–SiOx/Si surface also including the wide scan XPS spectrum (b) with high resolution spectra of the Si 2p region (c) the N 1s region (d) and the C 1s region (e).

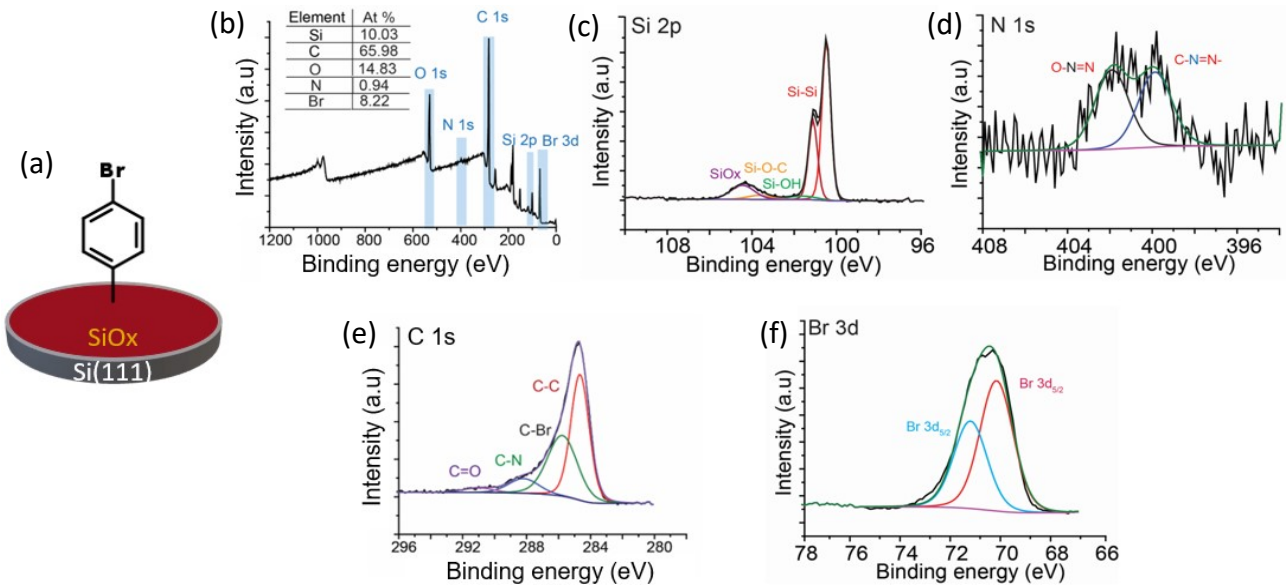

Fig S4. Schematic showing all XPS spectra collected for **2** on nat–SiOx/Si. (a) A schematic showing **2** attached to a nat–SiOx/Si surface with the wide survey XPS spectrum (b) and high resolution spectra for the Si 2p region (c) the N 1s region (d) the C 1s region (e) and the Br 3d region (f).

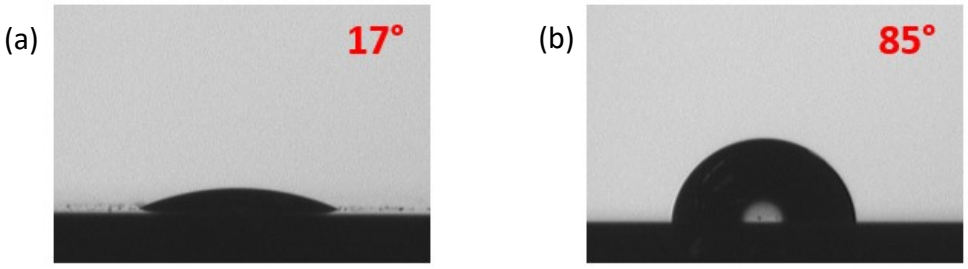

Fig S5. Representative images showing the contact angles for the bare surfaces of (a) nat–SiOx/Si and (b) Si–H.

Table S1. Contact angles for functionalised and bare surfaces along with their associated error. The error bars are the standard error from five different surfaces.

Sample	Water Contact Angle (θ)	
	Angle (°)	±
Silicon Hydride (Si - H)	84.9	2.8
Native SiOx on Silicon (nat-Si/SiOx)	17.6	1.6
1 on nat-Si / SiOx	45.4	2.8
2 on nat-Si / SiOx	92.1	2.6
3 on nat-Si / SiOx	85.2	3.0

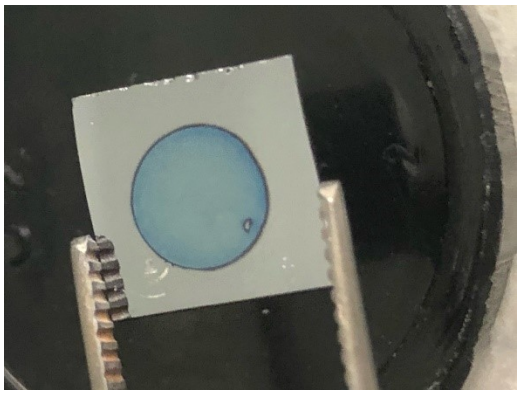

Fig S6. Image showing the organic film formed from **2** on nat–SiOx/Si, which is sufficiently thick to give a colour change visible by the naked eye

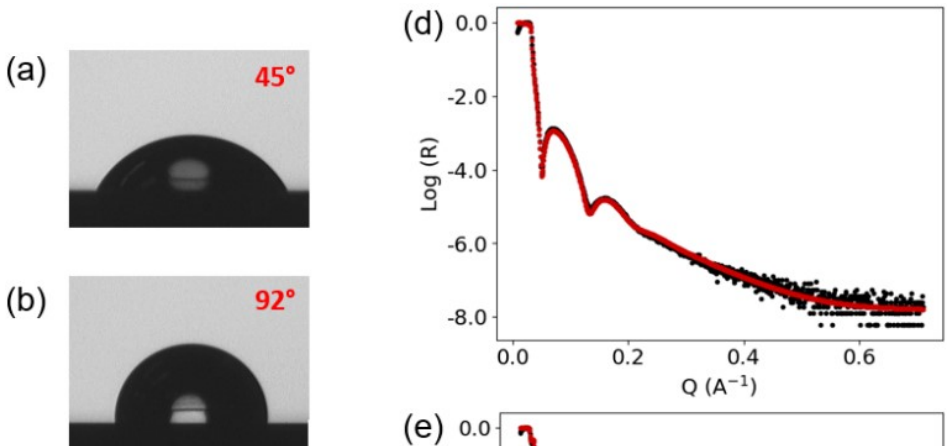

Fig S7. Schematic showing the water contact angles (WCA) and XRR spectra for various diazonium organic films on nat–SiOx/Si. The WCA values were averaged over a minimum of 5 surfaces. WCA measured on nat–SiOx/Si modified by molecule (a) **1**, (b) **2**, (c) **3**. XRR profiles (points with error bars) and corresponding fits to a single layer model (solid lines) of (d) **1**, (e) **2**.

Figure S7 presents the WCA and organic film thickness on nat–SiOx/Si, where figures 4a–4c show the WCAs of **1**–**3** respectively, each showing a significant difference from a bare nat–SiOx/Si surface which has a WCA of 18° (Fig. S5, ESI). The hydrophobic nature of **2** and **3** is caused by the end groups of each monomer (Br and heptane respectively) and the thickness of the organic film. Figures 4d and 4e show the x-ray reflectometry (XRR) spectrum for **1** and **2** on nat–SiOx/Si, which allows determination of the organic film thickness. The thickness of **1** on nat–SiOx/Si was 7.19 ± 0.04 nm. The thickness of **2** on nat–SiOx/Si was determined to be 194.3 ± 2.8 nm, which shows a significant difference from the organic film of **1**. The thickness of **2** is also significant enough to cause a colour change on the nat–SiOx/Si surface following the grafting procedure (Fig. S6, ESI). This is consistent with what has been observed in the AFM height imaging where the film that is formed from **2** showed a height which is five-folds higher than the film of **1**. The significant difference in the organic film thickness is explained by the structural nature of each diazonium salt, where **1** having two N_2^+ groups meaning that the molecules will have the possibility to connect with neighbouring molecules horizontally and produce dense polymeric structures that are well-packed on the surface, while **2** has one N_2^+ group and cannot bridge two of the neighbouring organic structures with the only possibility being the molecules add vertically to the existing polymer, resulting in branched-like structures and a thicker, more porous polymeric film (Fig. S7 and S8, ESI). This is consistent with the early current saturation of **1** in the voltammetric measurements (around the 3rd cycle) while with **2**, the reduction of the diazonium molecules continued even after 200 voltammetric cycles (Fig S2, ESI).

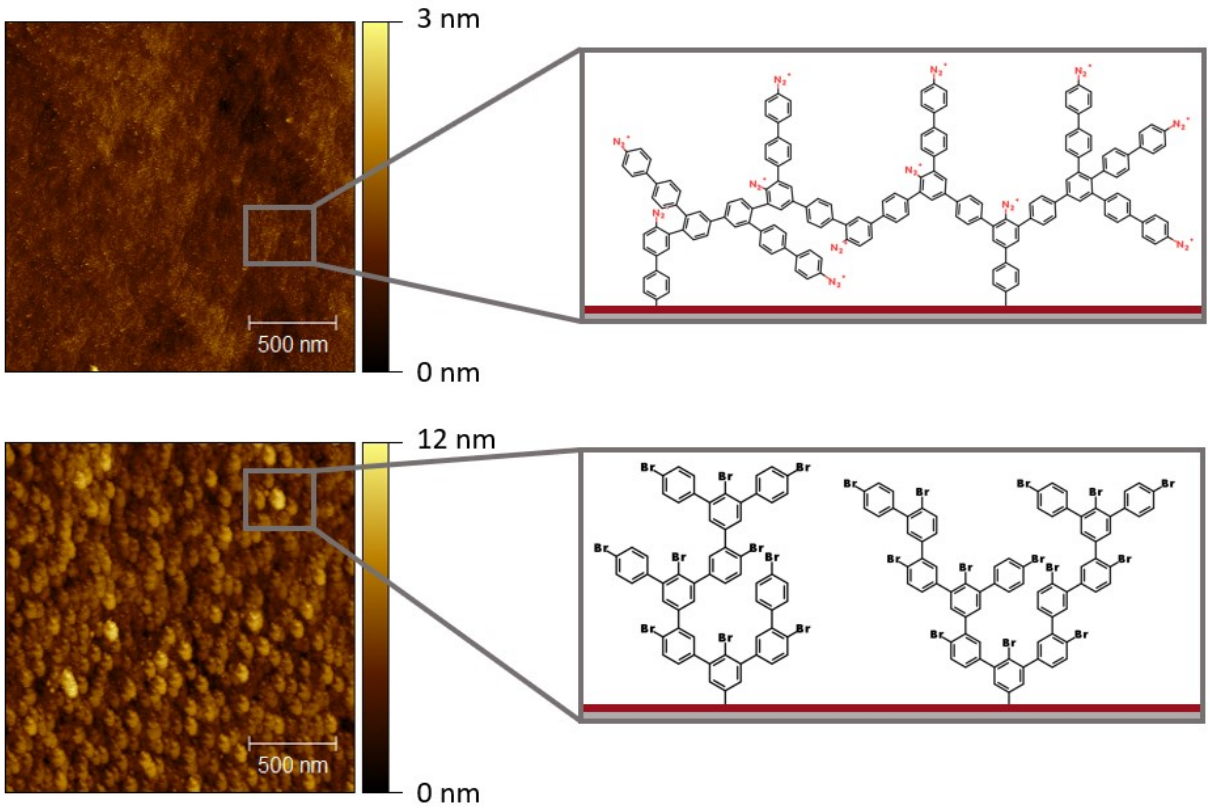

Fig S8. AFM topography images showing the organic films of **1** and **2**, with insets highlighting the structural differences between the two polymers. (a) AFM topography image of organic film **1**, showing a dense organic film with no significant features, indicating one interconnected structure which blocks further reduction after only three voltammetric cycles. (b) AFM topography image of the organic film formed from **2**, showing a very porous structure , which is attributed to polymeric chains with absence of bonding between the individual sprouts, where there are significant height differences which allow continuous reduction despite 300 voltammetric cycles.

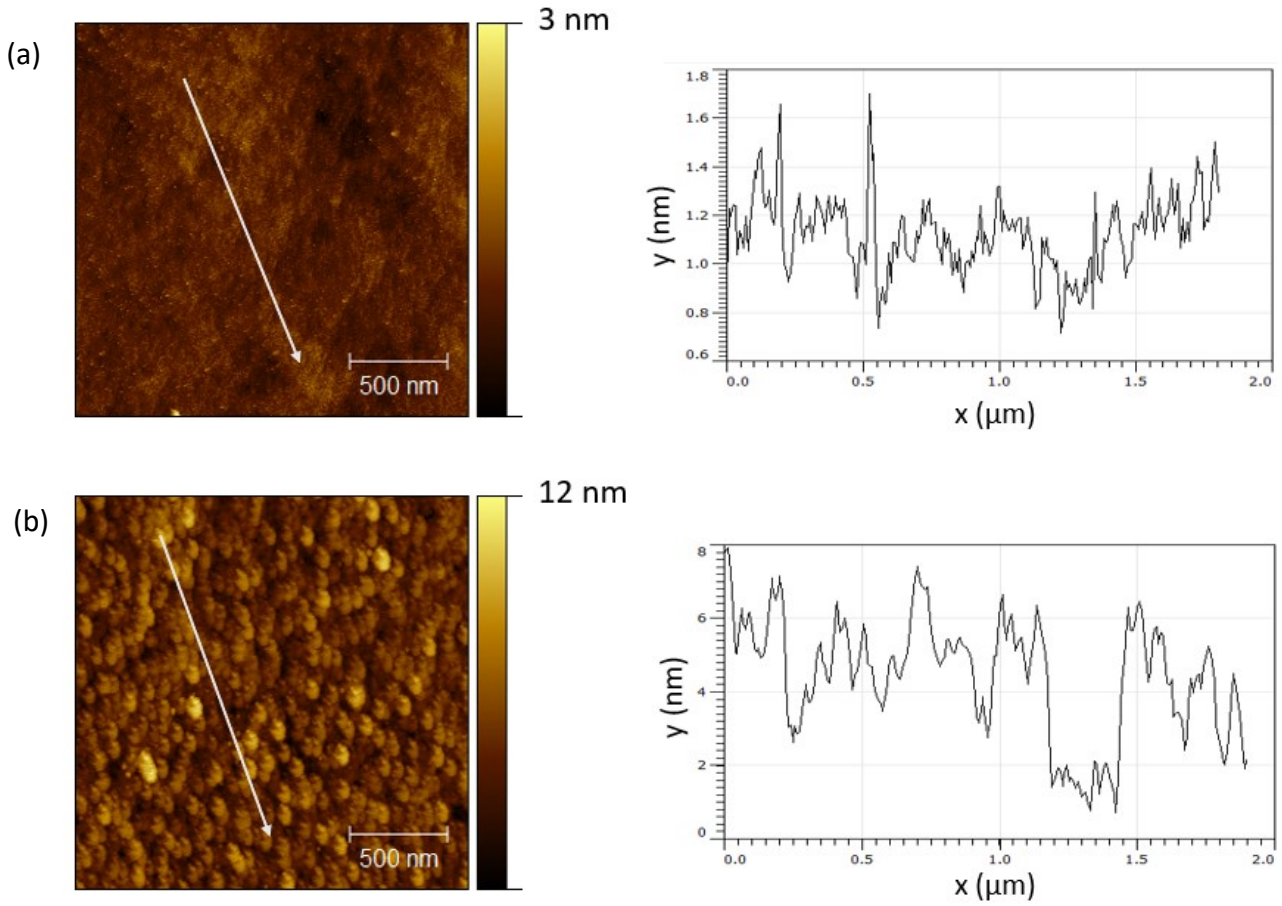

Fig S9. AFM topography images of the organic films formed from **1** and **2** with their associated height profiles (following the white arrow). (a) AFM topography image of organic film **1**, where the height plot shows little change in height between any features across the film. (b) AFM topography image of the organic film formed from **2**, showing notable height changes throughout the molecular film, indicating a porous structure which does not block further reduction effectively, thus allowing voltammetric cycling to show reduction waves for significantly longer time than that observed with the organic film of **1**.

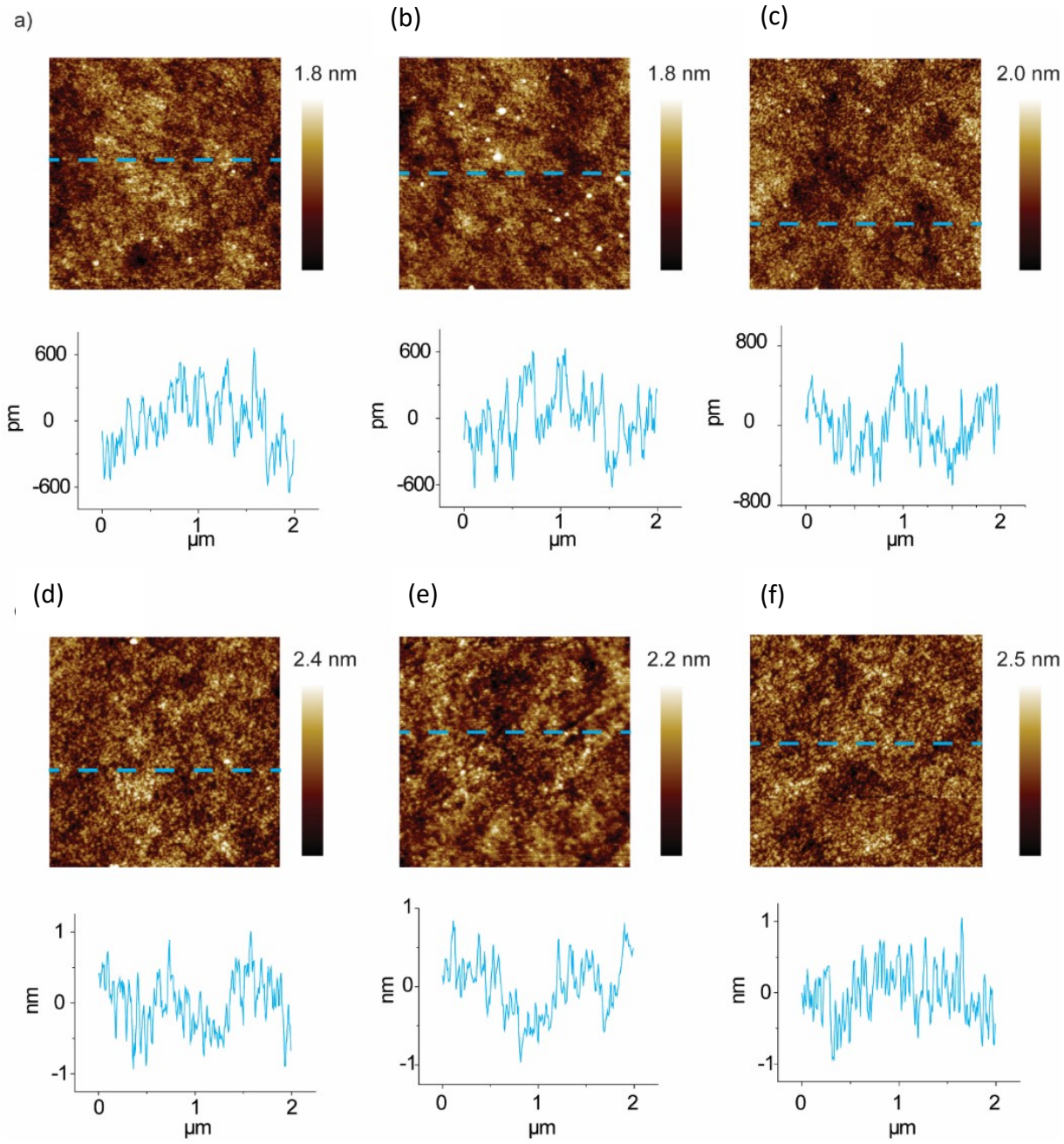

Figure S10. (a-c) AFM topography of the nat–SiOx/Si surface, (d-f) AFM topography of 20 nm silica/Si surface

surface. The insets show cross-sectional profile (line) roughness of the surfaces.

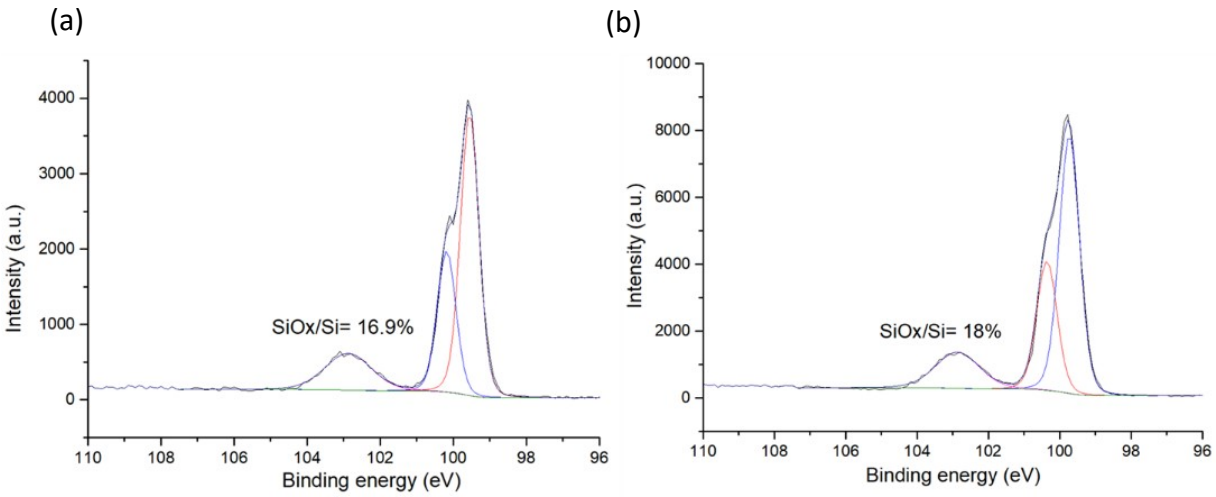

Figure S11. High resolution Si 2p region from different nat–SiOx/Si surfaces and atomic percentage of SiOx relative to Si for each surface.

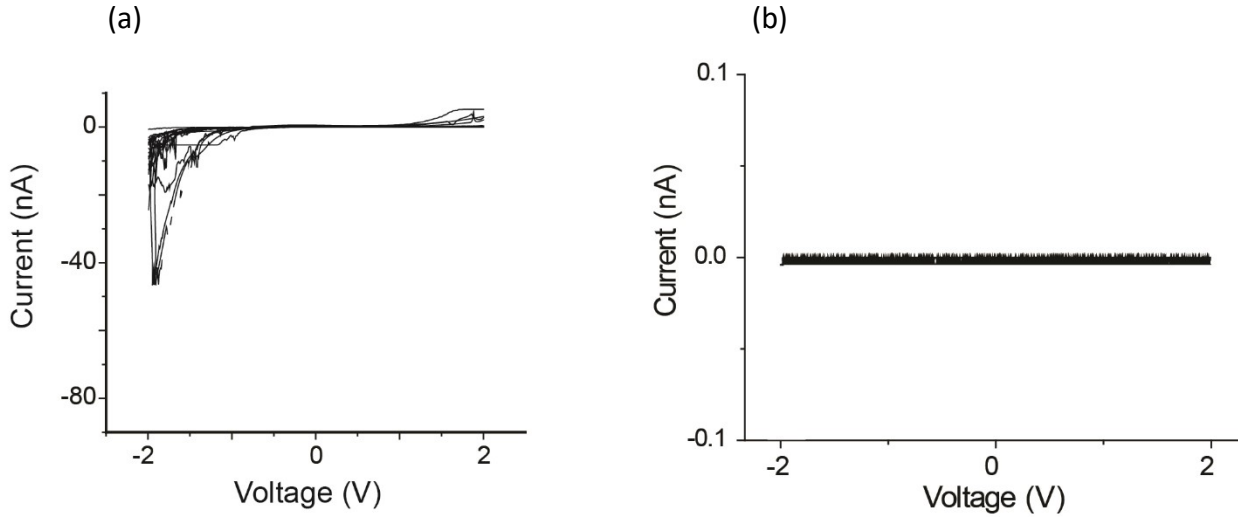

Figure S12. Current-voltage plots of (a) nat–SiOx/Si and (b) 20 nm silica/Si.

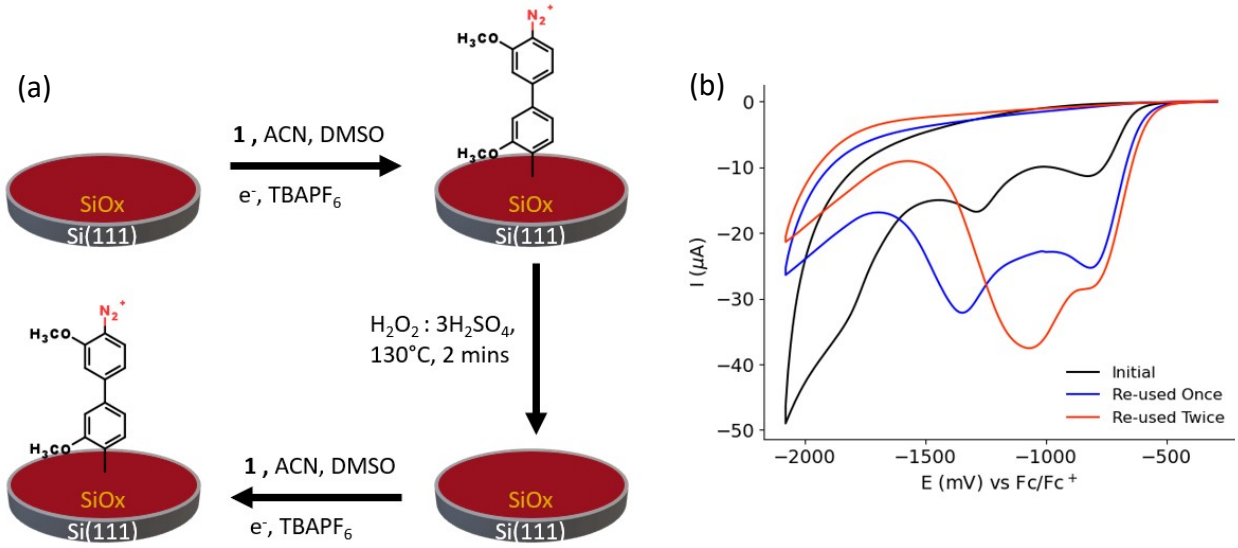

Fig S13. A reaction scheme and plot showing how nat–SiOx/Si surfaces can be re-used for electrochemical grafting experiments. (a) A simple reaction scheme showing the process off re-using nat–SiOx/Si surfaces for electrochemistry and (b) the associated cyclic voltammetry plots for a nat–SiOx/Si surface which was re-used twice.

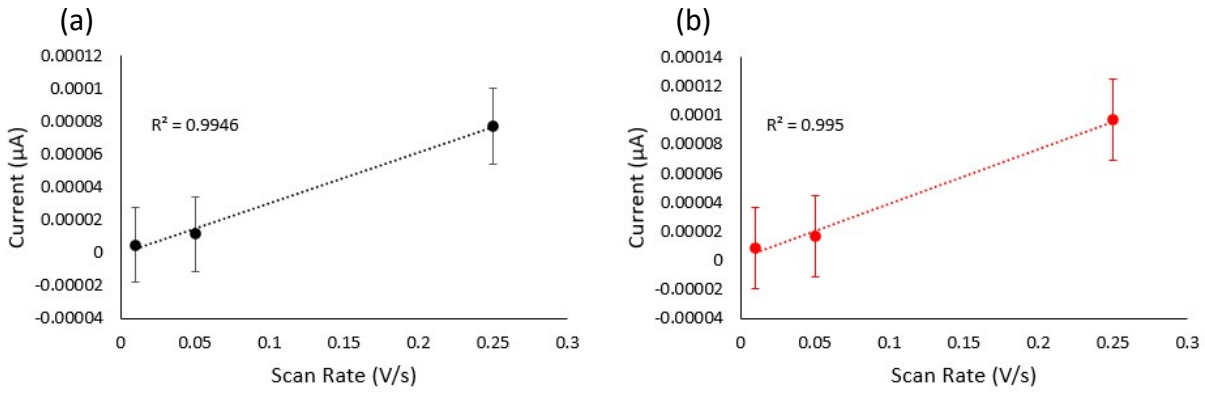

Fig S14. Current versus scan rate plots for each peak of molecule **1** at (a) -800 mV and (b) -1400 mV where each shows a linear trend of current vs scan rate indicating an adsorption based mechanism.

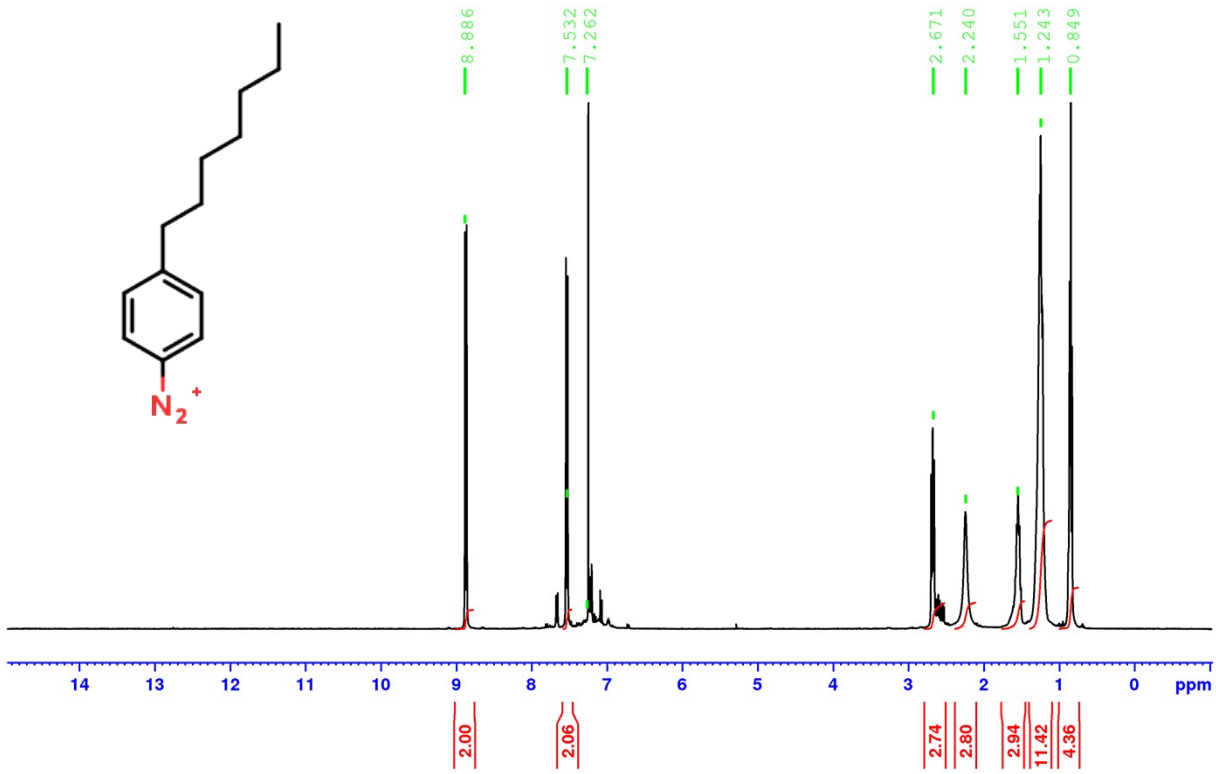

Fig S15. ^{1}H NMR spectrum of 4-heptylbenzene diazonium, 400 MHz ($CDCl_3$). δ 8.89 (m, 2H), 7.53 (m, 2H), 2.67 (t, *J* = 7.8 Hz, 3H), 2.24 (s, 3H), 1.55 (m, 3H), 1.24 (m, 11H), 0.85 (m, 4H).

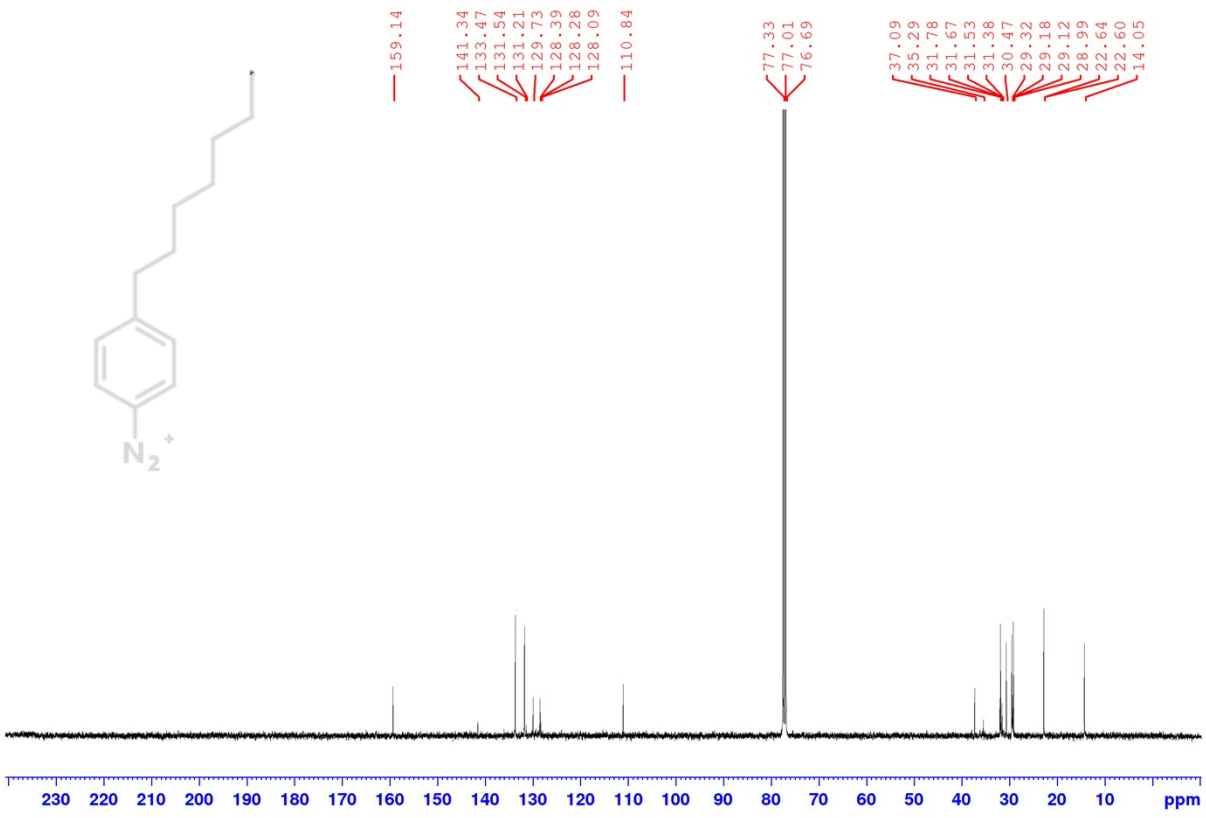

Fig S16. ^{13}C NMR spectrum of 4-heptylbenzene diazonium, 75 MHz ($CDCl_3$). δ CN 159.1, CH 133.5, CH 131.5, CH 129.7, CH 128.4, C 110.84, CH_2 37.1, CH_2 35.3, CH_2 31.8, CH_2 30.5, CH_2 29.3, CH_2 22.6, CH_3 14.1.

Table S2. Fitted organic film thickness and surface roughness (in nm), fitted SLD (in 10^{-6} nm^{-2}) for **1** and **2** on nat–SiOx/Si by electrochemical grafting as determined by XRR data (XRR spectra in Figure 4 of the main text).

Sample	Thickness / nm	Fitted SLD / × 10^{-6} nm^{-2}	Air-monolayer / monolayer-surface roughness / nm	Volume Fraction	Molecules per cm^2
1 on nat-Si/SiOx	7.19 ± 0.04	0.126 ± 0.0006	1.191 / 0.274	0.783 ± 0.004	5.47 ± 0.04 × 10 ^22
2 on nat-Si/SiOx	194.35 ± 2.85	0.116 ± 0.0017	0.32 / 2.11	0.630 ± 0.009	3.52 ± 0.07 × 10^24

Experimental Section

Materials

Unless specified otherwise, all chemicals were of analytical grade and used as received. The solvents, acetonitrile (ACN), dichloromethane (DCM), dimethyl sulfoxide (DMSO) and isopropanol were all distilled before use. MIlliQ water (>18 MΩ cm) was used for surface cleaning, glassware cleaning and for the preparation of the electrolyte solutions. The sulfuric acid (Puranal TM, 96 %), hydrogen peroxide (30 wt % in H_2O) and ammonium fluoride (Puranal TM, 40 wt % in H_2O) were of semiconductor grade and used for silicon-wafer cleaning and etching. Fast B Blue Salt (97 %), 4-bromobenzene diazonium (96 %), ferrocene carboxylic acid (99 %), N,N'-dicycohexycarbodiimide (DCC, 99 %) and N,N'-dimethylpyridin-4-amine (DMAP, 99 %) were used as purchased from Sigma Aldrich. 4-heptylbenzene diazonium was synthesised from 4-heptylaniline (98 %) using a standard literature procedure.(1) The silicon wafers were purchased from Siltronix, S.A.S. (Archamps, France). The silicon wafer used were n-type phosphorus doped with a resistivity of 0.007–0.013 Ω cm^{-1} and a thickness of 500 ± 25 μm and were $\langle 111 \rangle$ oriented. The 20 nm thick silica on silicon wafers were purchased from Siltronix, S.A.S. (Archamps, France). This oxide layer was thermally grown on n-type silicon wafers with a thickness of 500 micrometres.

Surface Modification

Preparation of Native Silica on Silicon

The nat–SiOx layer need not be removed and thus the preparation involves only cutting the silicon wafers into smaller pieces (approx. 1 cm × 1 cm) then washing sequentially in DCM, isopropanol and water before any surface modifications.

Preparation of Si–H surfaces

The preparation of Si–H followed a previously reported procedure.(2, 3) In brief, silicon wafers were cut into pieces (approximately 1 × 1 cm), cleaned in hot Piranha solution (130 °C, 3:1(v/v) mixture of concentrated sulfuric acid to 30% hydrogen peroxide) for 20 minutes, then rinsed with water and etched in deoxygenated (40 wt%) aqueous ammonium fluoride solution under a stream of argon for 13 minutes. The etched samples were rinsed with Milli–Q water and DCM before further functionalisation.

Steglich esterification of ferrocene carboxylic acid with silanol groups

N,N–Dicyclohexylcarbdiimide (DCC) (5 mM, DCM), 4–dimethylaminopyridine (DMAP) (1 mM, DCM) and ferrocene carboxylic acid (5 mM, DCM) were cooled to 0°C. Each of the nat–SiOx/Si electrodes were prepared according to the above procedure. After cooling the solutions, DCC and the ferrocene carboxylic acid was added to each electrode, and then left to cool to 0°C. After 10 minutes, the DMAP was added, leaving each of the electrodes in the dark for 48 hours. The surfaces were then removed from the reaction solution and washed in DCM before immediately being characterised using the electrochemical techniques.

Diazonium Synthesis

Synthesis of 4-heptylbenzene Diazonium from 4-heptylaniline

4-heptylaniline (100 mg) was dissolved in minimal hydrochloric acid (3 M, 4.2 mL) while being cooled to 0°C. An equimolar solution of sodium nitrite (0.0361 g) was prepared in minimal MilliQ water and cooled to 0°C. The $NaNO_2$ solution is slowly added dropwise to the 4-heptylaniline solution while being maintained at 0°C. Once all is added, a saturated solution of zinc chloride (0.196 g in MilliQ water) is added with occasional stirring. After the mixture was left for 10 minutes at 0°C, the entire solution is filtered and the collected solid is washed several times with small portions of cold ethanol and anhydrous ether. The product was then dried under vacuum yielding 0.165 g (84%) of product. (1)

Surface Characterisation

Electrochemical measurements

Electrochemical measurements were carried out in a single-compartment, three-electrode PTFE cell using a CHI650 electrochemical workstation (CH Instruments, USA). The modified silicon surface served as the working electrode, a platinum wire as the auxiliary electrode, and an Ag/AgCl aqueous electrode (1.0 M KCl, CH Instruments, USA) as the reference electrode. The counter electrode is switched out for an Ag/AgCl 'leakless' electrode (3.4 M, KCl) when performing experiments in ACN. The Ag/AgCl 'leakless' electrode is calibrated against a ferrocene solution (1 mM) before any electrochemistry experiments.

Atomic Force Microscopy (AFM) Measurements

All the topography imaging were conducted on Bruker Dimension FastScan atomic force microscopy in air and at room temperature. All the AFM data was processed with NanoScope Analysis.

The antimony (n) doped silicon tips (TESPA-V2, Bruker AFM Probes), with spring constant of 42 N/m and resonance frequency of 320 kHz, were used to probe the sample topography. The measurements were performed in tapping mode while the size of image was set to 2×2 μm^2, the resolution to 256 points/line and the scan rate to 0.5 Hz.

X-Ray Photoelectron Spectroscopy (XPS) Measurements

X-ray photoelectron spectroscopy (XPS) analysis of the monolayer-modified silicon surfaces was performed on a Kratos Axis Ultra DLD fitted with a monochromatic Al Kα (hυ1486.6 eV) radiation source operating at 150 W, and a hemispherical analyzer (165 mm radius) running in fixed analyzer transmission mode. The photoelectron take-off angle was normal to the sample, and the chamber operated at 7 $\times 10^{-9}$ Torr. The analysis area was 300 × 700 µm, and an internal flood gun was used to minimize sample charging. Survey spectra (accumulation of three scans) were acquired between 0 and 1100 eV, with a dwell time of 100 ms, a pass energy of 20 eV, and a step size of 0.1 eV. High-resolution scans (accumulation of 10 scans) used a pass energy of 20 eV, and a step size of either 0.05 eV (Si 2p, 90–110 eV), or 0.1 eV (C 1s, 277–300 eV). XPS data were processed in CasaXPS (version 2.3.18) and any residual charging was corrected by applying a rigid shift to bring the main C 1s emission (C–C) to 285.0 eV.

Contact angle analysis

The wettability of the Si surfaces was measured by an automated static water contact angle with a Krüss DSA 100 goniometer. The reported values are the average of at least three droplets, and the error bars represent the standard deviation of three measurements on three different surfaces.

X-Ray Reflectivity (XRR) Measurements

X–ray reflectivity was conducted at the solid-air interface on a Panalytical Ltd X'Pert Pro instrument with a tube source (Cu Kα radiation, λ = 1.54 Å). The X–ray beam was focussed using a Gödel mirror with fixed slits of 0.1 mm. A motorised stage housed the sample throughout the measurements, with angles measured from 0.05° to 5.00° in 0.01° steps for 20 seconds per step. The raw data was processed using in house software, where the critical edge was processed to a reflectivity of unity, and data was presented as reflectivity versus momentum transfer, Q,

$$Q = \frac{4\pi \sin(\theta)}{\lambda}$$

Where λ is the X-ray wavelength and θ is angle of incidence. Further data analysis utilised the *refnx* software package.(4) The organic layer was described as a single slab defined by its thickness, scattering length density (SLD) and roughness. These parameters were varied along with background value using a least-squares regression using a differential evolution algorithm until the fit matched the collected data.

References

1. Hodgson HH. The Sandmeyer reaction. Chem Rev. 1947;40(2):251-77.

2. Ciampi S, Eggers PK, Le Saux G, James M, Harper JB, Gooding JJ. Silicon (100) electrodes resistant to oxidation in aqueous solutions: an unexpected benefit of surface acetylene moieties. Langmuir. 2009;25(4):2530-9.
3. Ciampi S, Böcking T, Kilian KA, James M, Harper JB, Gooding JJ. Functionalization of acetylene-terminated monolayers on Si (100) surfaces: a click chemistry approach. Langmuir. 2007;23(18):9320-9.
4. Nelson ARJ, Prescott SW. refnx: neutron and X-ray reflectometry analysis in Python. J Appl Crystallogr. 2019;52(1):193-200.